

A Statistical Framework for Forecasting Cumulative Dose Metrics in Adaptive Radiotherapy

Robert Boyd^{1,2} and Wolfgang A. Tomé^{1,2,*}

¹Montefiore Einstein, 111 East 210th Street, Bronx, NY 10467

²Institute for Onco-Physics, Albert Einstein College of Medicine, 1300 Morris Park Ave, Bronx, NY 10461

Abstract

Adaptive radiation therapy (ART) seeks to maintain accurate dose delivery by monitoring anatomical changes during treatment and modifying plans accordingly, yet commonly used approaches for estimating cumulative dose rely on heuristic, deterministic assumptions and do not quantify uncertainty in future dose delivery. We present a statistical framework based on simple exponential smoothing (SES) to forecast cumulative dose metrics probabilistically throughout the course of ART. Adapting lead-time SES methods from inventory control, we model cumulative dose trajectories and derive closed-form prediction intervals and threshold exceedance probabilities for clinically relevant dose metrics. The framework was evaluated using per-fraction dose–volume histogram data recomputed on daily volumetric imaging for 32 prostate and 19 head-and-neck patients, allowing assessment of empirical interval coverage, interval width, and adaptive decision support performance. SES-based forecasts demonstrated robust coverage probabilities across a range of smoothing parameters and provided appropriately scaled uncertainty estimates for remaining-course cumulative dose. In addition, a difference-based formulation enabled in-course estimation of the probability that an adaptive plan would improve delivered dose metrics relative to the original plan. This SES-based forecasting approach offers a computationally efficient and statistically grounded method for anticipating cumulative dose delivery, supporting quantitative, individualized adaptive monitoring and evidence-based replanning decisions within routine ART workflows.

Introduction

In 1997, Yan et al. formalized the concept of adaptive radiation therapy (ART) as a closed-loop process in which treatment is monitored with imaging during the course of therapy and the treatment plan is modified based on that feedback to maintain geometric accuracy and conformal dose delivery.¹ Subsequently, Yan and colleagues used portal imaging (and later CT) to characterize patient-specific prostate setup and motion and design patient-specific PTVs, enabling margin reduction and potential sparing of normal tissues.² With the advent of IMRT, steep dose gradients in head-and-neck treatment plans prompted the use of repeat CT (re-CT) imaging during treatment to quantify large, systematic anatomic changes such as primary and nodal tumor regression, parotid shrinkage, and treatment-related weight loss.³⁻⁹ Serial re-CT–based replanning studies showed that mid- or multiple-course adaptive replanning improved target and OAR DVHs compared with continuing the original plan on the re-CT anatomy.¹⁰⁻¹²

*Email: wolfgang.tome@einsteinmed.edu

Today, ART is commonly implemented with daily IGRT volumetric imaging and dose-of-the-day accumulation to quantify what has been delivered and decide when replanning thresholds are met. Commercial platforms (e.g., systems supporting rigid/deformable image registration, dose warping and accumulation, and automated reporting/flags) have made these workflows increasingly feasible in routine clinical practice. The lack of consensus on ART strategy has led to an ad-hoc collection of heuristic methods for estimating final dose accumulation. Two commonly used summary strategies are last-observation-carried-forward (LOCF), which presumes that the most recently delivered fraction dose will continue for the remainder of the course,¹³ and as-plan-forward (APF), which presumes that the planned fraction dose will persist.¹⁴ These approaches generally depend on point estimates of past and current dose and do not provide a formal quantification of uncertainty in future daily doses under either the current or an adapted plan.

Exponential smoothing (ES) forecasting methods offer a well-defined framework for predicting future dose trajectories for individual treatments. ES models, in particular simple exponential smoothing (SES), are attractive because they are computationally efficient, accommodate evolving local trends, and can be updated sequentially as new fractions are delivered. Also known as Exponentially Weighted Moving Average (EWMA), SES has been employed in the field of medical physics primarily through statistical process control¹⁵ of quality assurance and treatment delivery.¹⁶⁻²⁰ In this work we adapt lead-time ES forecasting,²¹⁻²² used predominantly in inventory control, to develop a SES cumulative dose model that provides analytic prediction intervals and probabilities for exceeding clinically relevant dose metric thresholds on a per-patient basis. Using per-fraction DVH data from dose-of-the-day calculations on daily images for prostate and head-and-neck treatments, we characterize the empirical coverage and interval width of these forecasts across a range of smoothing parameters, illustrate their use for adaptive monitoring of dose metric constraints, and demonstrate a difference-based formulation for quantifying in-course the probability that an adaptive plan improves delivered dose metrics relative to the original plan. This framework can be integrated with existing ART workflows and provides a simple, statistical tool for anticipating future dose accumulation and guiding adaptive replanning decisions.

Mathematical Framework

SES Cumulative Dose Forecasting

Let y_s^{obs} denote the observed per-fraction dose delivered at treatment fraction $s = 1, 2, \dots$. At any time t , the information set $\mathcal{F}_t = \{y_1^{\text{obs}}, \dots, y_t^{\text{obs}}\}$ contains all doses delivered up to and including fraction t . For a delivery horizon of h additional fractions, we define the *remaining-course* (lead-time) cumulative dose as the random variable

$$Y_{t+h} = \sum_{j=1}^h y_{t+j}. \quad (1)$$

We denote point forecasts of future doses by a hat. In particular, $\hat{y}_{t+h|t}$ is the point forecast of y_{t+h} based on observed data \mathcal{F}_t , and

$$\hat{Y}_{t+h|t} = E(Y_{t+h} | \mathcal{F}_t) \quad (2)$$

is the corresponding forecast of the remaining-course cumulative dose. Throughout, E and V denote the conditional expectation and the variance conditioned on the observed information set \mathcal{F}_t . We use the simple linear innovations state space model

$$\begin{aligned} y_t^{\text{obs}} &= \ell_{t-1} + \varepsilon_t \\ \ell_t &= \ell_{t-1} + \alpha \varepsilon_t \end{aligned} \quad (3)$$

where ℓ_t is the level at time t , $0 < \alpha \leq 1$ is the smoothing parameter, and ε_t denotes the one-step forecast error (or innovation). In what follows it is always assumed that the one-step innovations ε_t are independent and identically distributed, following a normal distribution with mean zero and variance σ^2 . In the ARIMA(0,1,1) framework, SES is the optimal linear one-step-ahead forecast (see appendix).

The conditional mean of the cumulative dose at time $t + h$ is the sum of the point forecasts:

$$\hat{Y}_{t+h|t} = E(Y_{t+h} | \ell_t) = \sum_{j=1}^h \hat{y}_{t+j|t}. \quad (4)$$

For the simple linear innovations state space model, we are considering here this sum reduces to the following:

$$\hat{Y}_{t+h|t} = h\ell_t. \quad (5)$$

Each future innovation ε_{t+h-j} contributes once directly to y_{t+h-j} , and to each of the next j future fractions through the level update

$$\ell_{t+h-j} = \ell_{t+h-j-1} + \alpha \varepsilon_{t+h-j} \quad (6)$$

so, the same innovation is propagated into $y_{t+h-j+1}, \dots, y_{t+h}$, each time with coefficient α . Thus ε_{t+h-j} has total weight $1 + j\alpha$ in the remaining-course sum (1) which yields the factor $(1 + j\alpha)^2$ in the conditional variance. Therefore, the conditional variance of the cumulative dose is

$$V(Y_{t+h} | \ell_t) = \sigma^2 \sum_{j=0}^{h-1} (1 + j\alpha)^2. \quad (7)$$

Effecting the sum yields

$$V(Y_{t+h} | \ell_t) = \sigma^2 h \left[1 + \alpha(h-1) + \frac{\alpha^2}{6} (h-1)(2h-1) \right]. \quad (8)$$

For notational convenience let us define the following function of h :

$$\Omega(h) \equiv h \left[1 + \alpha(h-1) + \frac{\alpha^2}{6} (h-1)(2h-1) \right], \quad (9)$$

then the conditional variance simply becomes,

$$V(Y_{t+h} | \ell_t) = \sigma^2 \Omega(h). \quad (10)$$

Although we have framed the development above in terms of an observed per-fraction dose and its remaining-course cumulative (lead-time) sum, the same lead-time SES framework extends directly to other measures that can be accumulated across fractions. For DVH-derived endpoints that are not additive (e.g., the volume receiving dose X , V_x), the clinically relevant target can be the average scaled value over a specified number of fractions rather than a cumulative sum; in this case, we forecast the remaining-course cumulative total under SES and then rescale by the number of fractions in the averaging window to obtain prediction intervals and threshold probabilities for the average metric.

Initial level

Using a simple, self-starting initialization, we take the initial SES level as the mean of the first five observations of each series,

$$\ell_0 = \frac{1}{5} \sum_{s=1}^5 y_s, \quad (11)$$

This follows the usual self-starting SES approach, in which the recursive updates rapidly downweigh the influence of ℓ_0 , so that after a modest number of steps the effective forecast level is driven by later observed data.

Prediction interval

If we assume that the remaining-course cumulative dose Y_{t+h} given ℓ_t , denoted for notational convenience by $Y_{t+h} | \ell_t$, is approximately normal with mean $\hat{Y}_{t+h|t} = h\ell_t$ and variance $\sigma^2\Omega(h)$, then the central 95% prediction interval (PI) is given by:

$$PI = h\ell_t \pm z_{0.025} \hat{\sigma} \sqrt{\Omega(h)}, \quad (12)$$

where $\hat{\sigma}^2$ is the maximum likelihood estimate of the innovation variance σ^2 , which can be computed from the residuals (innovations) up to fraction t as follows,

$$\hat{\sigma}^2 = \frac{1}{t} \sum_{s=1}^t \varepsilon_s^2 \quad (13)$$

Likelihood estimate

To quantify the likelihood that the remaining-course cumulative dose stays below a clinically relevant threshold, we use the same normal approximation that underpins the prediction intervals above. Under SES with Gaussian innovations, the remaining-course cumulative dose satisfies

$$Y_{t+h} | \ell_t \approx \mathcal{N}\left(\hat{Y}_{t+h|t}, \hat{\sigma}^2\Omega(h)\right), \quad (14)$$

where $\hat{Y}_{t+h|t}$ is the SES point forecast of the remaining-course cumulative dose and $\hat{\sigma}^2$ is the maximum likelihood estimate of the innovation variance σ^2 up to fraction t (cf. equation (13)).

Since, Y_{t+h} is assumed to be approximately normally distributed with mean $\hat{Y}_{t+h|t}$ and variance $\hat{\sigma}^2\Omega(h)$, for any prescribed threshold d_{thr} on the remaining-course cumulative dose, the probability that the cumulative dose remains below this threshold is given by:

$$P(Y_{t+h} \leq d_{\text{thr}} | \ell_t) \approx \Phi\left(\frac{d_{\text{thr}} - \hat{Y}_{t+h|t}}{\hat{\sigma} \sqrt{\Omega(h)}}\right), \quad (15)$$

where Φ denotes the standard normal cumulative distribution function.

If the clinical constraint is expressed on the final total dose D_{max} , with $S_t = \sum_{s=1}^t y_s^{\text{obs}}$ already delivered, we find for $d_{\text{thr}} = D_{\text{max}} - S_t$, and substituting this in the above expression yields:

$$P(Y_{t+h} \leq D_{\text{max}} - S_t | \ell_t) \approx \Phi\left(\frac{D_{\text{max}} - (S_t + \hat{Y}_{t+h|t})}{\hat{\sigma} \sqrt{\Omega(h)}}\right). \quad (16)$$

While, the assumption of independent, identically distributed Gaussian innovations has been invoked solely to obtain closed-form expressions for prediction intervals and threshold probabilities, previous work analyzing the setup corrections derived from 3800 daily image registrations using volumetric imaging has shown that setup errors appear to be normally distributed making this also a reasonable assumption.⁸ However, alternatively uncertainty may also be quantified using an implicit, non-parametric approach via a residual bootstrap. In this formulation, historical innovations are resampled and propagated through the SES recursion to generate an empirical predictive distribution for the remaining-course cumulative dose. Prediction intervals and pass/fail probabilities are then extracted directly from this simulated distribution, without requiring explicit distributional assumptions on the innovations. In practice, approximately 5,000 simulated paths are sufficient to obtain stable prediction intervals and exceedance probabilities (Hyndman et al.²³, Chapter 6).

Adaptive plan comparison

Let plan 1 be the *current* plan and plan 2 the *adaptive* plan. For fractions $s = 1, \dots, t$, let $D_{1,s}$ and $D_{2,s}$ be the dose per-fraction values for plan 1 and plan 2, respectively. We now define a lower-is-better dose metric as follows

$$\Delta_s = \begin{cases} D_{1,s} - D_{2,s} < 0 & \text{Plan 1 has lower dose} \\ D_{1,s} - D_{2,s} > 0 & \text{Plan 2 has lower dose} \end{cases} \quad (17)$$

Using the SES model described above, we treat $\{\Delta_s\}$ as a single time series and obtain an approximate normal distribution for the final total difference between the two plans,

$$C_{\Delta,t}(r) \approx N(\mu_{\Delta}, \sigma_{\Delta}^2), \quad (18)$$

where r is the number of remaining fractions, and μ_{Δ} and σ_{Δ}^2 are the SES forecast mean and variance for the cumulative difference.

Since, $\Delta_t = \text{current plan} - \text{adaptive plan}$, a positive final difference $C_{\Delta,t}(r) > 0$ means the adaptive plan has a lower total dose. The probability that the adaptive plan is better is given by

$$P_{\text{adaptive}} = P(C_{\Delta,t}(r) > 0) = 1 - P(C_{\Delta,t}(r) \leq 0) = 1 - \Phi\left(-\frac{\mu_{\Delta}}{\sigma_{\Delta}}\right) = \Phi\left(\frac{\mu_{\Delta}}{\sigma_{\Delta}}\right) \quad (19)$$

$$P_{\text{adaptive}} = \Phi\left(\frac{\mu_{\Delta}}{\sigma_{\Delta}}\right),$$

where Φ is the standard normal cumulative distribution function and the last equality is true by symmetry of the normal distribution.

Methods

Prediction interval and hit rate

Time-series data were collected retrospectively from fraction-dose calculations for 32 prostate (PST) and 19 head-and-neck (HN) radiotherapy treatments. MiM ART Assist (MiM Software Inc., Cleveland, OH) was used to manage the acquisition of daily cone-beam CT (CBCT) images and subsequent image processing. Synthetic CT (sCT) images were generated from CBCT, planning CT contours were propagated, and fractional dose was recalculated on the sCT using MiM SureCalc (SciMoCa Monte Carlo) commissioned to our clinical linear accelerator beam models. From each fractional dose distribution, dose–volume histogram (DVH) data were exported and processed using an in-house Python pipeline to extract the per-fraction mean dose to the organs at risk (OARs) listed in Table 1, yielding one mean-dose time series per OAR per patient for analysis.

Site	OARs
Prostate	Rectum, Bladder, Sigmoid, Femoral Head
Head-and-neck	Parotid, Spinal Cord, Larynx, Mandible, Submandibular, Esophagus, Oral Cavity

Table 1. List of OARs used for analysis of PI and hit rate.

For each OAR, let $\{y_t\}_{t=1}^N$ denote the observed per-fraction dose metric over N delivered fractions. We evaluated empirical prediction-interval coverage (“hit rate”) and prediction-average interval width for remaining-course cumulative-dose forecasts over horizons $h = 5i$, where $i \in \{1, \dots, 4\}$, and SES smoothing parameters $\alpha \in \{0.1, 0.2, \dots, 1.0\}$.

For a given horizon h (number of remaining fractions), the forecast origin was defined as $t_0 = N - h$, so that $\{y_t\}_{t=1}^{t_0}$ constitutes the observed data and $\{y_t\}_{t=t_0+1}^N$ the remaining-course segment. To make prediction-interval widths comparable across patients and OAR structures, each series was normalized by an approximate full-course total computed from the observed mean,

$$\tilde{D}(t_0) = \frac{N}{t_0} \sum_{t=1}^{t_0} y_t, \quad (20)$$

and

$$y_t^* = \frac{y_t}{\tilde{D}(t_0)}. \quad (21)$$

With this scaling, the cumulative dose through the forecast origin satisfies

$$\sum_{t=1}^{t_0} y_t^* = \frac{t_0}{N}, \quad (23)$$

and interval widths are reported in dimensionless units. This normalization is used solely to enable cross-series comparison; in a clinical setting, forecasts and prediction intervals would be reported in physical dose units.

For each (h, α) pair, SES was applied to the normalized observations $\{y_t^*\}_{t=1}^{t_0}$ via Eq. (3) with the self-starting initialization in Eq. (11). Under SES, $\hat{y}_{t_0+j|t_0} = \ell_{t_0}$ for $j = 1, \dots, h$, hence the forecast mean of the remaining-course cumulative dose is $\hat{Y}_{t_0+h|t_0} = h \ell_{t_0}$ (cf. Eq. 5) and the conditional variance was estimated as $V(Y_{t_0+h} | \ell_{t_0}) = \hat{\sigma}_{t_0}^2 \Omega(h)$ (cf. Eq. 10), where $\hat{\sigma}_{t_0}^2$ is computed from one-step residuals up to t_0 (see Eq. (13)). From this the central 95% prediction interval is formed, $PI = h\ell_{t_0} \pm z_{0.025} \hat{\sigma}_{t_0} \sqrt{\Omega(h)}$ (cf. Eq. 12).

The realized remaining-course cumulative dose (normalized units) is given by

$$S_h^*(t_0) = \sum_{j=1}^h y_{t_0+j}^*. \quad (24)$$

For each forecast instance (i.e., each time series evaluated at a given horizon), we recorded (i) whether the realized value $S_h^*(t_0)$ lies inside the prediction interval and (ii) the prediction-interval width, $W = PI_{95}^{\text{upper}} - PI_{95}^{\text{lower}}$. For each (h, α) pair, the empirical hit rate was computed as the pooled proportion of hits, and the mean prediction-interval width was computed by averaging W across the same pooled set of forecast instances.

Adaptive monitoring

As a proof-of-concept, we evaluated two parotid gland mean-dose time series, each representing the per-fraction mean dose over an entire treatment course. Let y_t denote the parotid mean dose at fraction t , for $t = 1, \dots, n$. The two examples were chosen to illustrate contrasting behaviors: one series shows substantial day-to-day variation with only a modest change in level halfway through the course, while the other has relatively low short-term variability but a pronounced mid-course shift in level. For each series we applied SES ($\alpha = 0.3$) in equation (3) and obtained the SES level ℓ_t ; the raw data y_t and the corresponding ℓ_t (scaled by the total number of fractions n) were plotted together to show how the smoothed level tracks the underlying trend.

We then focused on forecasting the final course-averaged mean dose using prediction intervals. At each fraction t , we formed the cumulative sum $S_t = \sum_{k=1}^t y_k$ and the running mean $m_t = \frac{S_t}{t}$, and plotted the running mean scaled by n to represent its implication for the full course. The simple exponential smoothing state model fit to (y_1, \dots, y_t) provides the predictive distribution for the remaining cumulative dose $\sum_{k=t+1}^n y_k$, with predictive mean $\mu_t^{\text{fut}} = h\ell_t$ and lower/upper bounds

$L_t^{\text{fut}} = h\ell_t - z_{0.025} \hat{\sigma} \sqrt{\Omega(h)}$ and $U_t^{\text{fut}} = h\ell_t + z_{0.025} \hat{\sigma} \sqrt{\Omega(h)}$ (cf. equations (5), (9), and (12)), where $h = n - t$ denotes the number of remaining fractions. The corresponding prediction for the final mean dose can then be written as

$$\bar{y}_n \approx \frac{1}{n}(S_t + h\ell_t), \quad (25)$$

Separating the contribution from the delivered and remaining fractions, as

$$\mu_{\text{final},t} = \frac{t}{n}m_t + \left(1 - \frac{t}{n}\right)\ell_t, \quad (26)$$

the associated prediction interval for the final mean dose is

$$\left[\frac{1}{n}(S_t + L_t^{\text{fut}}), \frac{1}{n}(S_t + U_t^{\text{fut}}) \right], \quad (27)$$

which we plotted after scaling and centering around the sum of delivered and expected remaining dose to illustrate how uncertainty about the final mean dose evolves over the course.

Finally, we translated these prediction intervals into likelihood-style plots for two illustrative tolerance thresholds designed to simulate “pass” and “fail” scenarios. For each series, we defined a symmetric band around the observed dose level whose width was proportional to the empirical variability of the data (for example, using a multiple of the standard deviation of per-fraction or differenced doses), thereby obtaining lower and upper tolerance levels T_{low} and T_{high} . Assuming a normal approximation for the predictive distribution of \bar{y}_n , the model provides, at each fraction t , an estimated probability $P(\bar{y}_n \leq T \mid y_1, \dots, y_t)$ for each threshold $T \in \{T_{\text{low}}, T_{\text{high}}\}$. These probabilities were plotted over the course for both SES and LOCF (implemented by setting the SES smoothing parameter $\alpha = 1$, so that the forecast equals the most recent observation), allowing a direct comparison of how quickly and reliably each approach discriminates between pass and fail outcomes as more fractions are delivered.

Adaptive plan DVH evaluation

While we so far have formulated everything in terms of dose, our approach is equally applicable to more general dose metrics, as the following example for adaptive plan evaluation using dose volume metrics demonstrates. To illustrate the use of SES for adaptive decision making, we retrospectively analyzed a single prostate patient treated with an initial pelvic plan to 45 Gy in 25 fractions for whom an adaptive plan was generated and compared against the initial plan. The rectum was identified as an organ-at-risk due to an increase in fractional volume receiving high dose (35-45 Gy). A new plan was generated to reduce rectal dose and was implemented on fraction 13. For this study, rectal contours from deformation mapping onto daily images for fractions 1-12 were manually reviewed and corrected to ensure geometric accuracy.

To quantify evidence that the adaptive plan improved rectal sparing, we applied the SES difference-based framework described above. For this example, we consider a dose volume objective, i.e., let $M_t^{(1)}(D)$ and $M_t^{(2)}(D)$ denote the per-fraction rectal volume receiving dose $\geq D$ (i.e., V_D) under the initial and adaptive plans, respectively. For each dose bin D , we define the difference series

$$\Delta_t(D) = \begin{cases} M_t^{(1)}(D) - M_t^{(2)}(D) < 0 & \text{Plan 1 offers improved sparing} \\ M_t^{(1)}(D) - M_t^{(2)}(D) > 0 & \text{Plan 2 offers improved sparing} \end{cases}, \quad (28)$$

i.e. positive values indicate improved rectal sparing using the adaptive plan, while negative values indicate worse rectal sparing using the adaptive plan.

Using data available through evaluation fraction $\tau = 12$, we applied SES ($\alpha = 0.3$) independently at each dose bin to the observed differences $\{\Delta_1(D), \dots, \Delta_\tau(D)\}$, yielding an SES level $\ell_\tau(D)$ and innovation variance estimate $\sigma^2(D)$ for each dose bin. The expected end-of-course DVH at total fraction number $N = 25$ was represented by the collection of SES levels across dose, i.e.,

$$\widehat{M}_N^{(k)}(D) = \ell_\tau^{(k)}(D), \quad k \in \{1,2\}, \quad (29)$$

where $\ell_\tau^{(k)}(D)$ is the SES level fitted to the per-fraction series $\{M_1^{(k)}(D), \dots, M_\tau^{(k)}(D)\}$ for plan k ($k = 1$ denotes the current plan, while $k = 2$ denotes the adaptive plan).

In parallel, under the SES-based normal approximation for the final cumulative between-plan difference,

$$\Delta_{\text{final}}(D) \sim \mathcal{N}\left(\mu_{\Delta,\tau}(D), \sigma_{\Delta,\tau}^2(D)\right), \quad (30)$$

we computed for each dose bin the probability that the adaptive plan was superior at the end of the course:

$$P(D) = \Pr(\Delta_{\text{final}}(D) > 0 \mid \Delta_1(D), \dots, \Delta_\tau(D)) = \Phi\left(\frac{\mu_{\Delta,\tau}(D)}{\sigma_{\Delta,\tau}(D)}\right), \quad (31)$$

where $\Phi(\cdot)$ as before is the standard normal cumulative distribution function. These probabilities were evaluated across dose bins and plotted as a function of dose to summarize where along the DVH the adaptive plan was most likely to improve rectal sparing relative to the initial plan.

Results

Prediction interval and hit rate

The 51 retrospective courses (32 prostate, 19 head-and-neck) and OARs shown in Table 1 did yield 261 time series for analysis of the mean prediction interval width vs horizon for varying α , the results of which are shown in Figure 1. For a fixed horizon, the prediction interval width increased monotonically with α . The width governed by the term $\sum_{j=0}^{h-1} (1 + j\alpha)^2$, which increases monotonically with α for $j > 0$, and the average one-step innovations. The smoothing parameter α controls how much each new innovation persists into future fractions. A larger α makes innovations propagate more strongly and thus increases short-lag autocorrelation, i.e., the innovations don't cancel out when one sums over the remaining course; instead, they reinforce each other increasing the variance of the cumulative dose forecast. For every α , the mean interval width increased monotonically with horizon, as expected when predicting over a longer remaining course. At $h = 5$, mean widths ranged from 0.01 to 0.035. By $h = 20$, the mean widths ranged from 0.03 to 0.22.

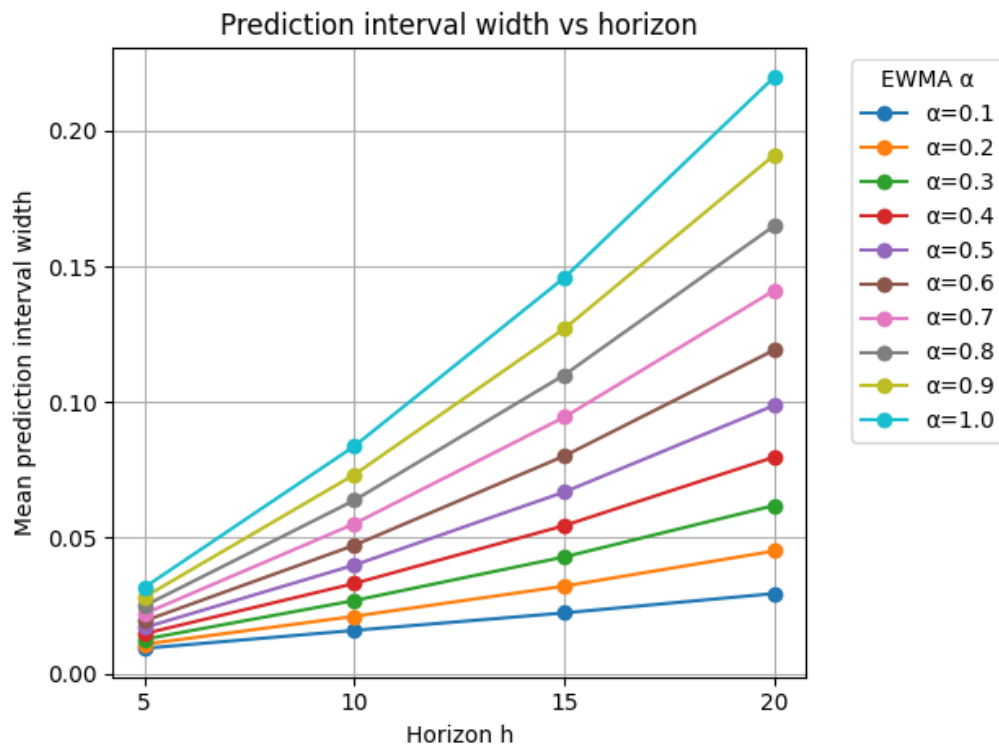


Figure 1. Mean prediction interval width vs horizon across α values.

Figure 2 shows the hit rate vs α . For very smooth models ($\alpha = 0.1$), coverage deteriorated markedly as the horizon increased: the hit rate fell from approximately 0.88 at $h = 5$ to around 0.74 at $h = 20$, well below the nominal 0.95 target. Slightly larger smoothing ($\alpha = 0.2$) improved coverage but still produced under-coverage, particularly at long horizons (hit rate ≈ 0.91 at $h = 20$). In contrast, $\alpha = 0.3$ did yield hit rates close to or slightly above the desired nominal target (roughly 0.95–0.98) at all horizons, while $\alpha \geq 0.4$ produced strongly conservative intervals with empirical hit rates very close to 1.0 across the board. Overall, moderate smoothing ($\alpha \approx 0.3$)

produced prediction intervals with empirical coverage closest to the nominal target level of 95%, whereas very small α values systematically underestimated uncertainty (under-coverage) and larger α values overestimated it (conservative over-coverage).

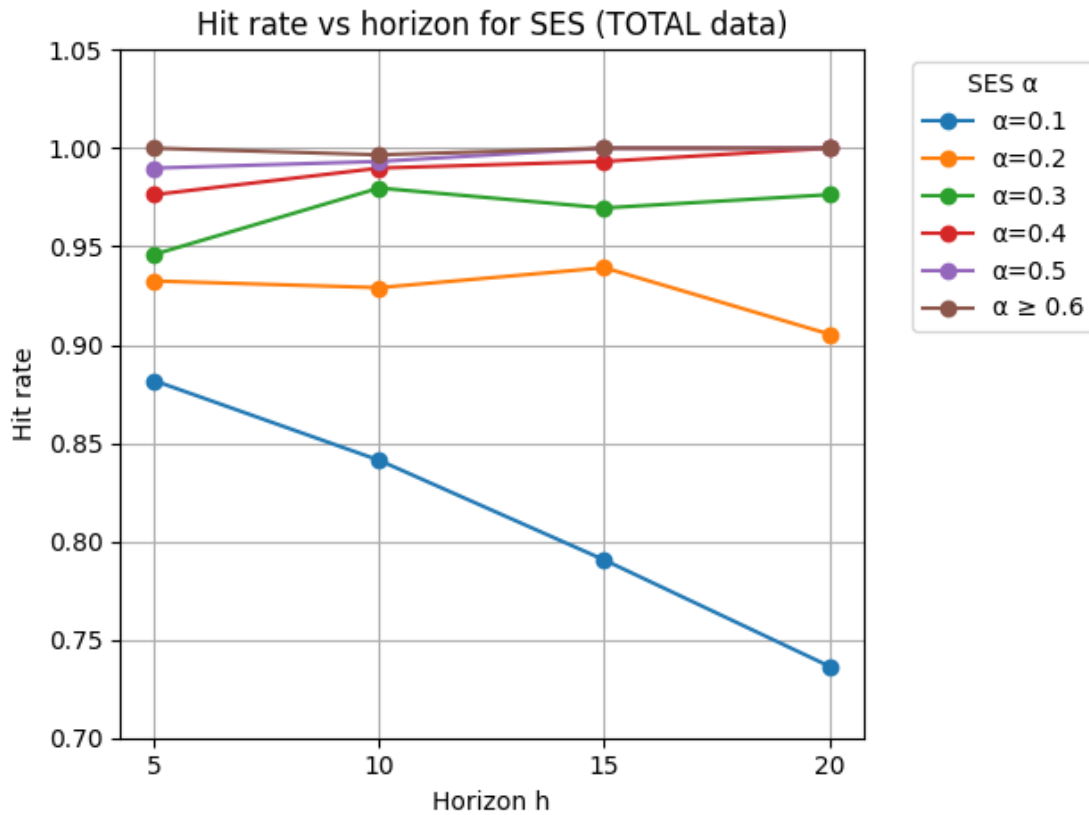


Figure 2. Hit rate vs horizon across α values.

Adaptive monitoring

To illustrate how SES forecasting behaves at the level of individual courses, we applied it to two parotid gland mean-dose time series selected to represent contrasting patterns of anatomical change and day-to-day variability in head-and-neck treatment. In the first example (cf. Figure 3), the per-fraction parotid mean dose exhibits substantial daily fluctuation with only a modest change in overall level roughly halfway through the course. The SES level tracks the underlying trend while substantially smoothing the high-frequency noise, providing a stable summary of the evolving dose history. When translated into a predictive distribution for the final course-averaged mean dose, the associated 95% prediction intervals are initially wide but contract gradually as more fractions are delivered, reflecting the model’s decreasing uncertainty about the eventual mean despite continued short-term volatility. For tolerance bands chosen to mimic clinical “pass” and “fail” criteria, the SES-based probabilities evolve smoothly over the course of treatment, with early fractions offering limited signal and later fractions driving the probabilities toward high or low exceedance likelihoods, depending on the realized trajectory. Relative to the LOCF baseline, the SES model yields less erratic and more definitive probability estimates, particularly in the presence of large day-to-day swings.

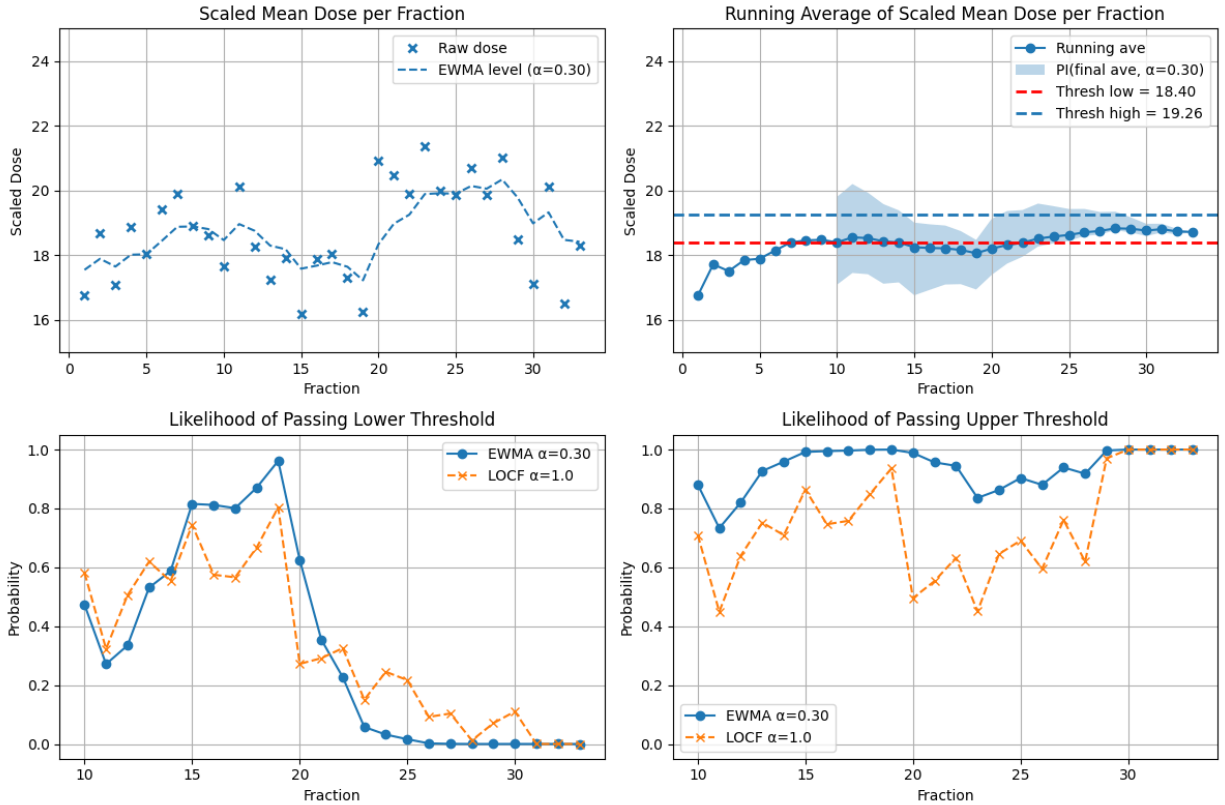


Figure 3. Adaptive monitoring: Mean parotid dose time series with significant daily variation. Note that monitoring starts at fraction 10. A sustained trend of decreasing values for the likelihood for a threshold in question indicate that the threshold will be crossed in the future.

The second example (cf. Figure 4) shows a parotid series with smaller daily variation but a pronounced mid-course shift in dose level, consistent with systematic anatomical change such as tumor regression or parotid shrinkage. In this case, the SES level adapts quickly once the shift begins, re-centering the forecast around the new regime after only a few fractions. The prediction intervals for the final mean dose narrow more rapidly than in Figure 3, because the lower within-course variability allows the model to infer the new level with fewer observations. The likelihood plots demonstrate that the SES-based probabilities for both “pass” and “fail” thresholds respond promptly to the change in trend, transitioning to near-certainty over a relatively small number of fractions. By comparison, LOCF responds more sluggishly, as it extrapolates the most recent individual fraction rather than the smoothed level, leading to slower and more oscillatory convergence of the implied probabilities. Taken together, Figures 3 and 4 show that SES can both stabilize noisy trajectories and remain sensitive to clinically meaningful shifts, providing a coherent probabilistic summary for adaptive monitoring.

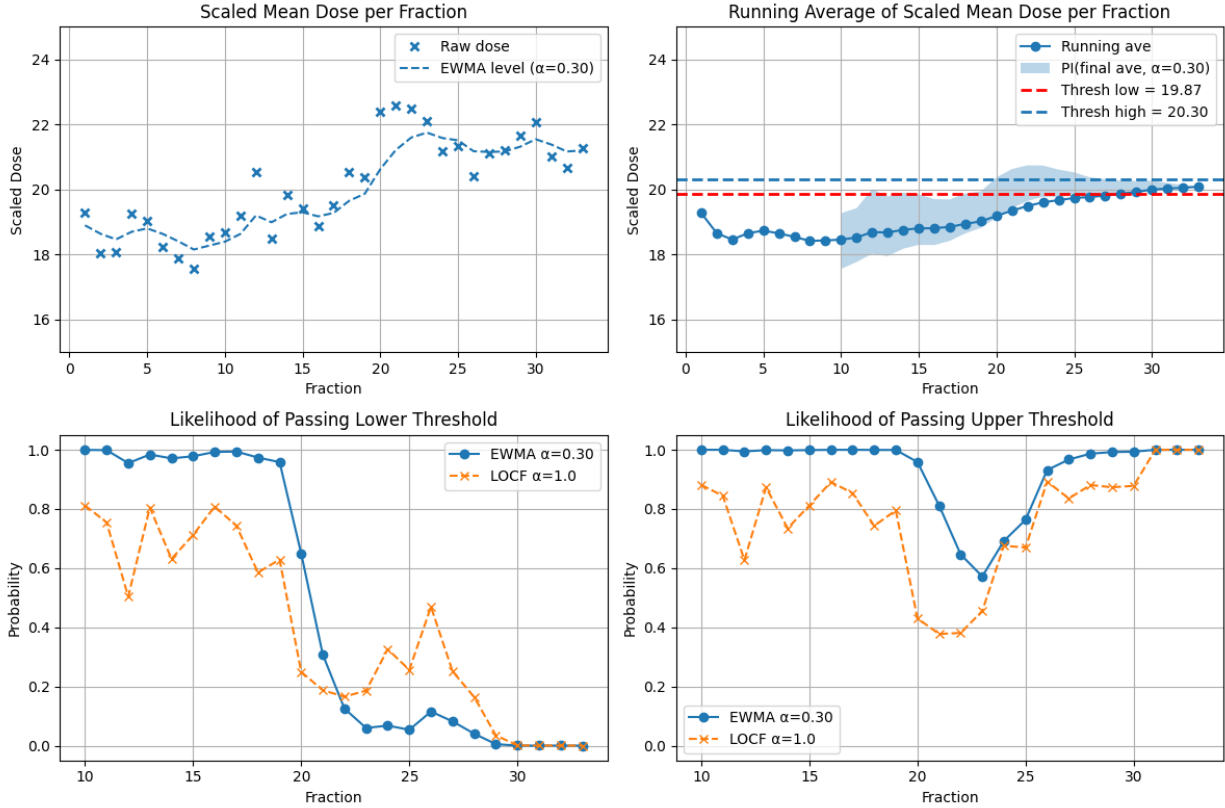


Figure 4. Adaptive monitoring: Mean parotid dose time series with smaller daily variation. Note that monitoring starts at fraction 10. A sustained trend of decreasing values for the likelihood for a threshold in question indicate that the threshold will be crossed in the future.

Adaptive plan DVH evaluation

Using data available through evaluation fraction $\tau = 12$ (with $N = 25$ planned fractions and $\alpha = 0.3$), the SES level DVHs shown in Fig. 5 indicate a dose-dependent tradeoff between the current plan and adaptive plan. The DVH curves cross near $D \approx 26$ Gy: below this point the adaptive plan shows a larger rectal volume receiving low-to-intermediate dose, whereas above this point the adaptive plan shows a consistently smaller rectal volume receiving intermediate-to-high dose. This pattern is in accordance with the adaptive planning intent to reduce rectal exposure in the 35–45 Gy range, where the adaptive SES-level DVH is visibly lower than the current-plan curve.

The corresponding SES difference-based probability curve, $P(D) = \Pr(\Delta_{\text{final}}(D) > 0 \mid \Delta_1(D), \dots, \Delta_\tau(D))$, confirms where the evidence supports improvement. Across the low-to-intermediate dose region (approximately 5–24 Gy), $P(D)$ is near zero, indicating strong evidence that the adaptive plan increases rectal volume at these doses relative to the current plan. In contrast, $P(D)$ rises rapidly in the crossover region (approximately 24–29 Gy) and remains near unity over most of the intermediate-to-high dose range (approximately 28–46 Gy), furnishing strong evidence that the adaptive plan reduces rectal volume receiving these higher doses. Deviations in the extreme high-dose tail occur where absolute rectal volumes are

very small and are therefore less clinically informative than the broad high-confidence improvement observed over the intermediate-to-high dose range. Using the same observed data through $\tau=12$, the LOCF-based probability curve (orange) is more conservative than SES—staying near 0.05–0.10 over roughly 5–21 Gy, rising more gradually through the crossover region (about 24–30 Gy), and then plateauing around ~ 0.9 (slightly below unity) across most of the 30–46 Gy range—still supporting adaptive improvement at intermediate-to-high doses but with reduced confidence relative to SES.

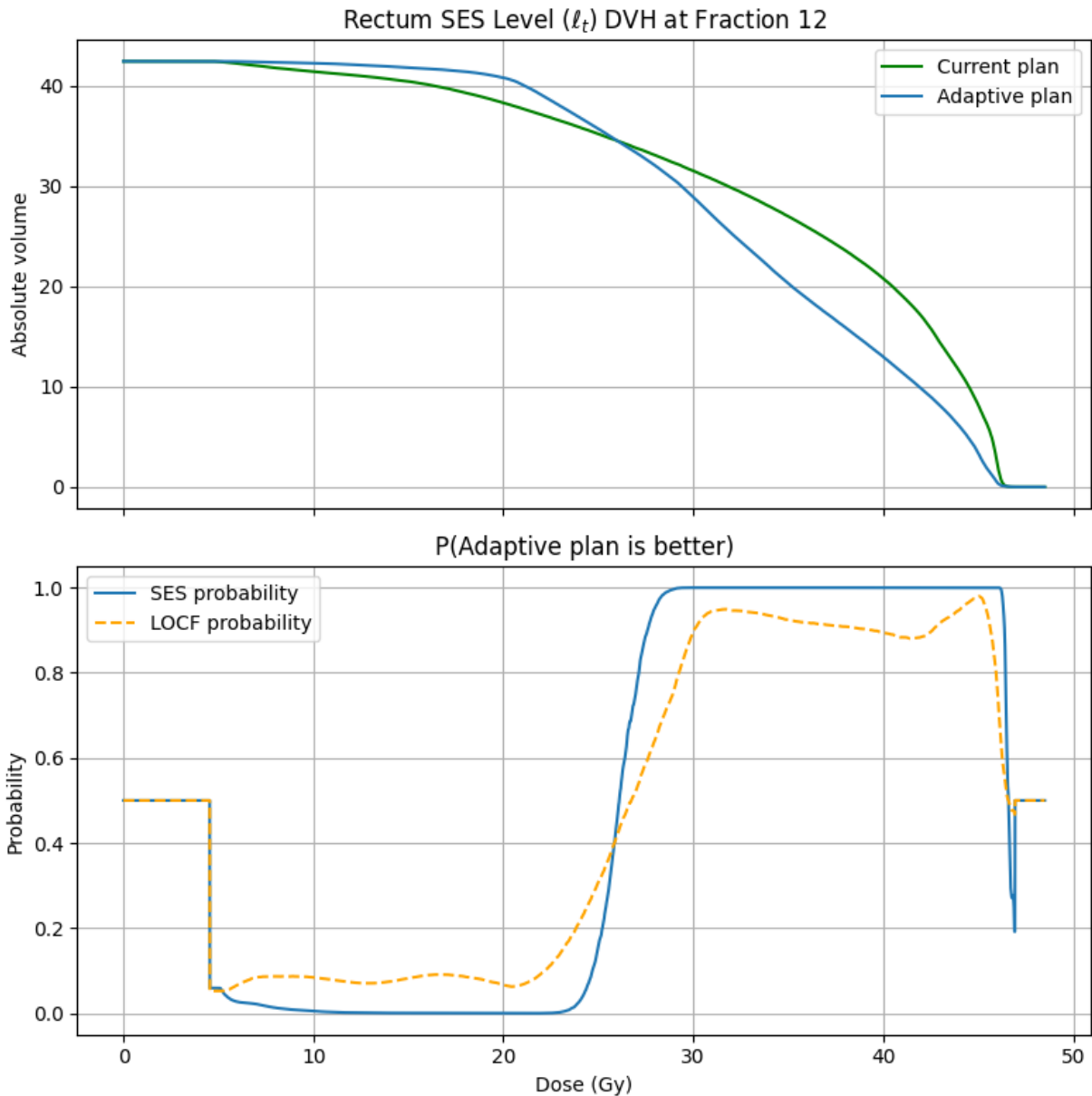


Figure 5. Plan comparison SES level DVH (top) between current (green) and adaptive (blue) plan at fraction 12, and probability that adaptive plan is better than current plan at different dose levels (bottom) for SES (blue) and LOCF (orange) forecasting.

Discussion

This work demonstrates that lead-time SES forecasting provides a practical statistical approach for monitoring delivered dose metrics and comparing adaptive plans in ART. Across 51 retrospective treatment courses (32 prostate, 19 head-and-neck), lead-time SES produced reasonably narrow prediction intervals for remaining-course cumulative dose with near-nominal empirical coverage under moderate smoothing ($\alpha \approx 0.3$) across a range of horizons. Case studies in parotid mean dose and rectal V_{45} further illustrated how SES can stabilize noisy daily trajectories, detect systematic shifts, and quantify the probability that a proposed plan will outperform the current plan for the dose metric in question.

ART is often described as a closed-loop process in which imaging feedback during treatment informs whether and when to replan. In current practice, however, this loop is usually closed with heuristic summaries such as LOCF, APF, or empirical means, which provide only point estimates and no explicit quantification of uncertainty in future dose. Here we instead cast dose evolution as a time-series forecasting problem using the notion of lead-time demand, with the remaining-course cumulative dose as the primary quantity of interest. Within this framework, SES is attractive because it provides simple closed-form expressions for the forecast mean and variance, so prediction intervals and probabilities can be updated analytically after each fraction.

The hit-rate and interval-width analyses provide empirical guidance for tuning the SES smoothing parameter. Small smoothing parameters ($\alpha \approx 0.05\text{--}0.10$) produced intervals that were too narrow, with coverage well below 95% as the horizon increased, indicating underestimated uncertainty. Large α values (> 0.5) gave overly conservative intervals with hit rates near 1.0 but substantially increased width. Moderate smoothing ($\alpha \approx 0.2\text{--}0.3$) offered a reasonable compromise, with near-nominal coverage across horizons and prediction intervals that remained a modest fraction of the normalized cumulative dose. This pattern is consistent with the role of α : larger values propagate innovations and increase the variance of the remaining-course sum, whereas smaller values dampen innovations but may miss real non-stationarity. From our experience, a single moderate α appears suitable as a practical default across sites and OARs, with future work focusing on data-driven tuning at the patient or structure level.

The parotid case studies illustrate two desirable properties of SES forecasting for adaptive monitoring of delivered dose metrics. First, the approach stabilizes noisy daily dose trajectories into smooth trend estimates and yields coherent likelihood plots. Second, it remains responsive to dosimetric shifts, adapting the forecast distribution for the final mean dose within only a few fractions when a systematic change occurs. In this setting, adaptive warnings and triggers could be defined in terms of the forecast probability of violating a constraint, with the likelihood function encoding how past fluctuations translate into uncertainty in the predicted final mean dose, rather than relying solely on a point forecast–threshold comparison. In contrast, the LOCF approach tends to chase noise, inflating early prediction intervals and yielding likelihoods in the 0.4–0.6 range, leaving adaptation decisions less definitive and closer to chance at the stage of treatment when adaptation could have the greatest impact.

The adaptive prostate plan example illustrates how the same SES framework can be used to compare competing plans in real time. By modeling per-fraction dose metric differences between

plans, the SES difference model yields a forecast distribution for the cumulative advantage of an adaptive plan, which in this case supported a high probability of benefit well before replanning occurred. Unlike APF-based approaches that rely on a single plan-derived point forecast, the SES prediction intervals use past fraction histories under each plan to quantify uncertainty in the remaining-course advantage. Extending this analysis across volume–dose levels revealed the expected inverse-planning trade-off, with strong support for the adaptive plan in the high-dose region and more neutral or unfavorable probabilities at lower doses. This perspective could be useful whenever multiple candidate adaptive plans are available, enabling probabilistic ranking rather than relying solely on static DVH comparisons.

This proof-of-concept study illustrates the flexibility of the SES framework and motivates broader investigations and validation studies. Beyond the simple univariate model considered here, higher-order ES, regressive ES with covariates, and vector ES for jointly modeling multiple dose metrics or other data can be embedded in the same lead-time forecasting formulation. Because the underlying recursions are computationally light, SES is efficient enough to be applied at the voxel level within reference-volume dose-accumulation ART methods.

The SES framework presented here assumes approximately Gaussian one-step innovations; in practice, dose fluctuations may be skewed or heavy-tailed, which can affect prediction-interval coverage under abrupt, systematic changes. In such settings, robust SES variants or nonparametric approaches (e.g., bootstrap-based prediction intervals) could better accommodate non-Gaussian behavior and improve predictive modeling.

In summary, this study shows that lead-time SES forecasting provides a simple way to quantify uncertainty in remaining-course cumulative dose and to translate daily dose-of-the-day data into clinically interpretable probabilities for both delivered dose metric monitoring and adaptive plan comparison. By moving to a probabilistic framework, this approach may provide a more systematic basis for ART decisions while remaining compatible with existing clinical workflows. As AI-based models for ART decision making enter the market, the SES framework can serve as a transparent statistical benchmark for validating and stress-testing black-box algorithms against observed data.

Conclusion

We have presented a simple SES-based framework to forecast remaining-course cumulative dose in adaptive radiotherapy, yielding closed-form point forecasts and prediction intervals, along with probabilities of exceeding clinical constraints and of benefit when comparing competing plans. In 51 retrospective prostate and head-and-neck treatment courses, the method yielded prediction intervals with near-nominal empirical coverage and improved upon a last-observation baseline; case studies further illustrated how it can support fraction-by-fraction monitoring of organs at risk and quantitative comparison of adaptive versus original plans. Because it is computationally efficient, this approach is readily implementable in existing ART workflows; future work will focus on larger-scale validation, data-driven selection of the smoothing parameter, exploration of robust innovation models, and prospective evaluation of decision rules for triggering replanning or choosing among adaptive strategies.

Appendix

We have modeled the observed per-fraction dose process $\{y_t\}$ using SES with level ℓ_t and smoothing parameter α , and we constructed forecasts and prediction intervals for the remaining-course cumulative dose by summing the point forecasts. We now show that this forecasting scheme is the optimal predictor for a nonstationary ARIMA(0,1,1) dose per fraction process $\{y_t\}$ whose level is allowed to fluctuate and an ARIMA(0,2,1) stochastic process for the nonstationary cumulative dose process $\{C_t\}$.

Let $\{z_t\}$ be an arbitrary nonstationary stochastic process, B the backshift operator defined by the functional equation $Bz_t = z_{t-1}$, and $\{\varepsilon_t\}$ independent innovations that are identically distributed with mean 0 and variance σ^2 . The linear stochastic process $\{\Delta_t\}$ given by

$$\Delta_t = \mu + \varepsilon_t + \psi_1\varepsilon_{t-1} + \psi_2\varepsilon_{t-2} + \dots$$

is stationary if $\sum_{i=0}^{\infty} |\psi_i| < \infty$. A nonstationary stochastic process $\{z_t\}$, for which the d -th difference of the process is stationary can be represented by the following model:

$$\phi(B)\Delta_t = \theta(B)\varepsilon_t, \text{ where } \Delta_t \equiv (1 - B)^d z_t \quad (\text{A1})$$

and

$$\phi(B) \equiv 1 - \phi_1 B - \phi_2 B^2 - \dots - \phi_p B^p \quad (\text{A2})$$

$$\theta(B) \equiv 1 - \theta_1 B - \theta_2 B^2 - \dots - \theta_q B^q \quad (\text{A3})$$

In practice, d is usually 0, 1, or at most 2, where $d = 0$ corresponds to the stationary behavior of the stochastic process. This class of processes are called *autoregressive integrated moving average* (ARIMA) processes of order (p, d, q) . The reason for inclusion of the word ‘integrated’ in ARIMA is as follows. Inverting $\Delta_t = (1 - B)^d z_t$ yields $z_t = S^d \Delta_t$, where $S = (1 - B)^{-1}$ is the *summation operator* defined by

$$S\Delta_t = \sum_{j=0}^{\infty} \Delta_{t-j} = \Delta_t + \Delta_{t-1} + \Delta_{t-2} + \dots$$

Thus, a general ARIMA process may be generated by summing or ‘integrating’ the process $\{\Delta_t\}$ d times.

In what follows let us denote by y_t the dose at fraction t , for which the difference in the delivered dose to the previous fraction is given by

$$\Delta_t = y_t - y_{t-1} = (1 - B)y_t. \quad (\text{A4})$$

Because the delivered per fraction is allowed to drift over the course of treatment, we treat the dose per fraction process $\{y_t\}$ as nonstationary but assume that the per-fraction differences dose process

$\{\Delta_t\}$ is a stationary process. Then $\{y_t\}$ can be modeled as an ARIMA(0,1,1) process which by (A1), (A2), and (A4) is given by:

$$(1 - B)y_t = (1 - \theta_1 B) \varepsilon_t, \quad (\text{A5})$$

where $|\theta_1| < 1$. Inverting, (A5) yields:

$$y_t = (1 - B)^{-1}(1 - \theta_1 B) \varepsilon_t, \quad (\text{A6})$$

Since $C_t = (1 - B)^{-1}y_t$, we find that

$$C_t = (1 - B)^{-2}(1 - \theta_1 B) \varepsilon_t, \quad (\text{A7})$$

Hence, with the assumptions we have made for the process $\{y_t\}$ this shows that the nonstationary cumulative dose $\{C_t\}$ process is an ARIMA(0,2,1) process. It can be shown that the process in (A6) can be written as the weighted average of previous values of the process:

$$y_t = \hat{y}_{t|t-1}(\alpha) + \varepsilon_t, \text{ where} \quad (\text{A8})$$

$$\hat{y}_{t|t-1}(\alpha) = \alpha \sum_{j=1}^{\infty} (1 - \alpha)^{j-1} y_{t-j} \quad (\text{A9})$$

and $\alpha = 1 - \theta_1$, hence $0 < \alpha < 2$ (cf. Ref. [24]). As discussed in Box et al.,²⁴ $\hat{y}_{t|t-1}(\alpha)$ is the optimal linear one-step-ahead predictor or level of the process $\{y_t\}$, i.e. what is known about the future value of this process. Using (A9) we now derive a recursive relationship for this optimal one-step-ahead predictor for y_t , which shows that $\hat{y}_{t|t-1}(\alpha)$ is indeed our simple SES model

$$\begin{aligned} \hat{y}_{t+1|t}(\alpha) &= \alpha \sum_{j=1}^{\infty} (1 - \alpha)^{j-1} y_{t-(j-1)} = \alpha \sum_{k=0}^{\infty} (1 - \alpha)^k y_{t-k} \\ \hat{y}_{t+1|t}(\alpha) &= \alpha y_t + \alpha \sum_{k=1}^{\infty} (1 - \alpha)^k y_{t-k} = \alpha y_t + (1 - \alpha) \alpha \sum_{k=1}^{\infty} (1 - \alpha)^{k-1} y_{t-k} \\ \hat{y}_{t+1|t}(\alpha) &= \hat{y}_{t|t-1}(\alpha) + \alpha [y_t - \hat{y}_{t|t-1}(\alpha)]. \end{aligned} \quad (\text{A10})$$

Setting $\ell_t = \hat{y}_{t+1|t}(\alpha)$ we find

$$\ell_t = \ell_{t-1} + \alpha (y_t - \ell_{t-1}), \quad (\text{A11})$$

This recursive relationship is easily derived from our SES state model shown in equation (3). Thus, our simple exponential smoothing of per-fraction doses model is the optimal linear one-step-ahead forecast under an ARIMA(0,1,1) model for the nonstationary dose per fraction process $\{y_t\}$ and an ARIMA(0,2,1) process for the nonstationary cumulative dose process $\{C_t\}$.

In the traditional SES setting one restricts $0 < \alpha \leq 1$, for which the SES level is an exponentially weighted moving average with nonnegative weights that sum to one. Although the SES–ARIMA(0,1,1) equivalence implies a broader admissible region $0 < \alpha < 2$ under invertibility, an $\alpha > 1$ yields alternating-sign weights, and therefore does not retain the standard smoothing interpretation; we therefore restrict ourselves to $0 < \alpha \leq 1$ for interpretability in ART. Also note that allowing the value $\alpha = 1$, shows that LOCF is one particular case of the SES strategy for adaptive monitoring we have discussed in this paper (cf. A11), since the level ℓ_t for any $t \in \{1, \dots, N\}$ is then simply equal to the observed value y_t .

References:

1. Yan D, Vicini F, Wong J, Martinez A. Adaptive radiation therapy. *Phys Med Biol*. 1997;42(1):123–132. doi: 10.1088/0031-9155/42/1/008
2. Yan D, Wong J, Vicini F, Michalski J, Pan C, Frazier A, Horwitz E, Martinez A. Adaptive modification of treatment planning to minimize the deleterious effects of treatment setup errors. *Int J Radiat Oncol Biol Phys*. 1997 Apr 1;38(1):197-206. doi: 10.1016/s0360-3016(97)00229-0.
3. Eisbruch A, Ten Haken RK, Kim HM, Marsh LH, Ship JA. Dose, volume, and function relationships in parotid salivary glands following conformal and intensity-modulated irradiation of head and neck cancer. *Int J Radiat Oncol Biol Phys*. 1999;45(3):577–587. doi: 10.1016/s0360-3016(99)00247-3.
4. Barker JL Jr, Garden AS, Ang KK, et al. Quantification of volumetric and geometric changes occurring during fractionated radiotherapy for head-and-neck cancer using an integrated CT/linear accelerator system. *Int J Radiat Oncol Biol Phys*. 2004;59(4):960–970. doi: 10.1016/j.ijrobp.2003.12.024.
5. Keller H, Tomé WA, Ritter MA, Mackie TR. Design of adaptive treatment margins for non-negligible measurement uncertainty: application to ultrasound-guided prostate radiation therapy. *Phys Med Biol*. 2004;49(1):69-86. doi:10.1088/0031-9155/49/1/005.
6. Mackie TR, Kapatoes J, Ruchala K, Lu W, Wu C, Olivera G, Forrest L, Tome W, Welsh J, Jeraj R, Harari P, Reckwerdt P, Paliwal B, Ritter M, Keller H, Fowler J, Mehta M. Image guidance for precise conformal radiotherapy. *Int J Radiat Oncol Biol Phys*. 2003 May 1;56(1):89-105. doi: 10.1016/s0360-3016(03)00090-7.
7. Mackie TR, Tomé WA. Advanced image-guided external beam radiotherapy. *Cancer Treat Res*. 2008;139:7-39. doi: 10.1007/978-0-387-36744-6_2.
8. Schubert LK, Westerly DC, Tomé WA, Mehta MP, Soisson ET, Mackie TR, Ritter MA, Khuntia D, Harari PM, Paliwal BR. A comprehensive assessment by tumor site of patient setup using daily MVCT imaging from more than 3,800 helical tomotherapy treatments. *Int J Radiat Oncol Biol Phys*. 2009;73(4):1260-1269. doi:10.1016/j.ijrobp.2008.11.054.
9. Tomé WA, Jaradat HA, Nelson IA, Ritter MA, Mehta MP. Helical Tomotherapy: Image Guidance and Adaptive Dose Guidance. *Front Radiat Ther Oncol*. 2006;40:162-178. doi:10.1159/000106034.
10. Hansen EK, Bucci MK, Quivey JM, Weinberg V, Xia P. Repeat CT imaging and replanning during the course of IMRT for head-and-neck cancer. *Int J Radiat Oncol Biol Phys*. 2006;64(2):355–362.
11. Ahn PH, Chen CC, Ahn AI, Hong L, Sripes PG, Shen J, Lee CC, Miller E, Kalnicki S, Garg MK. Adaptive planning in intensity-modulated radiation therapy for head and neck cancers: single-institution experience and clinical implications. *Int J Radiat Oncol Biol Phys*. 2011 Jul 1;80(3):677-85. doi: 10.1016/j.ijrobp.2010.03.014.

12. Gjini M, Ahmed S, Kalnicki S, Tomé WA, Garg MK, Kabarriti R, Brodin NP. Volumetric changes of the parotid gland during IMRT based on mid-treatment imaging: implications for parotid stem cell sparing strategies in head and neck cancer. *Acta Oncol.* 2022 Sep;61(9):1069-1074. doi: 10.1080/0284186X.2022.2110384.
13. Kainz K, Lim S, Chen GP, Li XA. *PreciseART® Adaptive Radiation Therapy Software: Dose Monitoring, Re-Planning, and Delivery Verification.* White paper. Sunnyvale, CA: Accuray Incorporated; 2017.
14. Byrne M, Archibald-Heeren B, Hu Y, et al. Varian ethos online adaptive radiotherapy for prostate cancer: Early results of contouring accuracy, treatment plan quality, and treatment time. *J Appl Clin Med Phys.* 2022;23:e13479.
15. Pawlicki T, Whitaker M, Boyer AL. Statistical process control for radiotherapy quality assurance. *Med Phys.* 2005;32(9):2777–2786. doi: 10.1118/1.2001209.
16. Sanghangthum T, Suriyapee S, Srisatit S, Pawlicki T. Retrospective analysis of linear accelerator output constancy checks using process control techniques. *J Appl Clin Med Phys.* 2013;14(1). doi: 10.1120/jacmp.v14i1.4032.
17. Pal B, Pal A, Das S, Palit S, Sarkar P, Mondal S, Mallik S, Goswami J, Das S, Sen A, Mondol M. Retrospective study on performance of constancy check device in Linac beam monitoring using statistical process control. *J Appl Clin Med Phys.* 2020;21(7). doi: 10.1016/j.rpor.2019.12.004.
18. Boyd R, Garg MK, Tomé WA. Non-stationary process control of fractionated treatment delivery. *Int J Radiat Oncol Biol Phys.* 2020;108(3):e347–e348.
19. Raveendran V, Rajendran GR, Anjana PT, et al. Moving towards process-based radiotherapy quality assurance using statistical process control. *Phys Med.* 2023;112:102651. doi: 10.1016/j.ejmp.2023.102651.
20. Xiao Q, Li G. Application and challenges of statistical process control in radiation therapy quality assurance. *Int J Radiat Oncol Biol Phys.* 2024;118(1):295–305. doi: 10.1016/j.ijrobp.2023.08.020.
21. Harrison, P. J. Exponential smoothing and short-term sales forecasting. *Management Science* 1967;13(11), 821–842. <https://doi.org/10.1287/mnsc.13.11.821>
22. Johnston, F. R. and P. J. Harrison. The variance of lead-time demand. *Journal of the Operational Research Society* 1986;37(3), 303–308. <https://doi.org/10.1057/jors.1986.48>
23. Hyndman, R.J., Koehler A.B., Ord J.K, and Synder R.D. *Forecasting with Exponential Smoothing: The State Space Approach.* Berlin Heidelberg: Springer Verlag; 2008.
24. Box, G.E.P., Jenkins, G.M. and Reinsel, G.C. *Time Series Analysis: Forecasting and Control.* 4th ed, Hoboken, NJ: Wiley; 2008.